Birchite $Cd_2Cu_2(PO_4)_2SO_4 \cdot 5H_2O$ as a model antiferromagnetic spin-1/2 Heisenberg J_1-J_2 chain

Masayoshi Fujihala,[1,2,*] Harald O. Jeschke,[3] Katsuhiro Morita,[4] Tomohiko Kuwai,[5] Akihiro Koda,[6] Hirotaka Okabe,[6] Akira Matsuo,[7] Koichi Kindo,[7] and Setsuo Mitsuda[2]

[1]*Advanced Science Research Center, Japan Atomic Energy Agency, Tokai-mura, Ibaraki 319-1195, Japan*
[2]*Department of Physics, Faculty of Science, Tokyo University of Science, Shinjuku, Tokyo 162-8601, Japan*
[3]*Research Institute for Interdisciplinary Science, Okayama University, Okayama 700-8530, Japan*
[4]*Department of Physics, Faculty of Science and Technology, Tokyo University of Science, Chiba 278-8510, Japan*
[5]*Graduate School of Science and Engineering, University of Toyama, Toyama 930-8555, Japan*
[6]*Muon Science Laboratory and Condensed Matter Research Center, Institute of Materials Structure Science, High Energy Accelerator Research Organisation, 1-1 Oho, Tsukuba 305-0801, Japan*
[7]*International MegaGauss Science Laboratory, Institute for Solid State Physics, The University of Tokyo, Kashiwa, Chiba 277-8581, Japan*

(Received 26 July 2022; revised 3 October 2022; accepted 15 November 2022; published 29 November 2022)

$S = 1/2$ Heisenberg J_1-J_2 chain antiferromagnets have been investigated extensively due to their exotic magnetic states. Here, we report the magnetic behavior of birchite $Cd_2Cu_2(PO_4)_2SO_4 \cdot 5H_2O$ and its effective spin model. Experimental studies by magnetic susceptibility, magnetization, heat capacity, and μSR measurements indicate the absence of long-range order down to 0.4 K. Theoretical studies reveal that birchite is a model compound for the J_1-J_2 antiferromagnetic chain: the intrachain interactions J_1 and J_2 are antiferromagnetic and their magnitude is about 100 times larger than the interchain interactions. The magnitude of J_2 is two to three times larger than that of J_1, thus the spin gap is expected to be only a few percent of that of J_1. The temperature dependence of the specific heat shows a broad peak at about 1 K ($\simeq 0.036 J_1$), which suggests the presence of a spin gap.

DOI: 10.1103/PhysRevMaterials.6.114408

I. INTRODUCTION

Frustrated one-dimensional (1D) magnets are excellent and versatile model systems in quantum many-body physics. The simplest frustration geometry in 1D magnets is the J_1-J_2 model,

$$\mathcal{H} = J_1 \sum_j \boldsymbol{S}_j \boldsymbol{S}_{j+1} + J_2 \sum_j \boldsymbol{S}_j \boldsymbol{S}_{j+2}, \quad (1)$$

where J_1 and J_2 represent nearest-neighbor and next-nearest-neighbor magnetic couplings, respectively [1]. In the case where J_2 is antiferromagnetic, i.e., $J_2 > 0$, the chain is frustrated, irrespective of the sign of J_1 [2]. The magnetic phase diagram of the $S = 1/2$ Heisenberg J_1-J_2 model for $J_1 > 0$ and $J_2 > 0$ has been studied extensively [3–6]. For $J_2/J_1 < 0.2411$, the ground state is expected to be a Tomonaga-Luttinger spin-liquid state. For $J_2/J_1 > 0.2411$, a spin gap opens and the chain is effectively in the dimerized state. At the Majumdar-Ghosh point ($J_2/J_1 = 0.5$), an exact ground state is represented by a superposition of spin singlets [1]. For $0.56 \leqq J_2/J_1 \leqq 1.25$, a magnetization plateau appears at $\frac{1}{3}$ of the full moment [4]. For $J_1 < 0$ and $J_2 > 0$, the spin state is significantly different from the case when both the J_1 and J_2 couplings are antiferromagnetic. In the quantum case, as in the classical case, the transition occurs at $J_2/J_1 = -0.25$ [7]. For $J_2/J_1 > -0.25$, the incommensurate correlations are long range in the classical case, whereas it is expected to be short range in the quantum case [8]. The gap is expected to be exponentially small and the nature of the ground state is not well understood. In high fields just below the saturation magnetization, a transition to quantum multipolar states such as a spin nematic phase occurs [9].

There are only a few ideal J_1-J_2 chain magnets with negligibly small interchain interactions; examples are the spin-Peierls system $CuGeO_3$ [10,11], the titanium alum $KTi(SO_4)_2 \cdot H_2O$ [12,13], the zigzag chain compound $(N_2H_5)CuCl_3$ [14–16], the host of a spin-nematic phase $LiCuVO_4$ [17–23], the frustrated spin chain compound linarite $PbCuSO_4(OH)_2$ [24–28], the ferromagnetic chain material $NaCuMoO_4(OH)$ [29–31], and the frustrated spin-1/2 chain compound β-$TeVO_4$ [32–34]. Interchain interactions are known not only to induce three-dimensional magnetic ordering, but also to have a significant effect on spin states in a magnetic field [35]. In many J_1-J_2 chain magnets, the nearest-neighbor magnetic couplings J_1 are superexchange interactions through Cu-O-Cu bonds, and J_2 are next-nearest-neighbor magnetic couplings through Cu-O-O-Cu bonds [10,11,17–31]. The magnitude of the interchain interactions and the ratio of next-nearest-neighbor coupling to nearest-neighbor coupling, J_2/J_1, is basically revealed only after synthesis. There are no clear guidelines for searching candidate compounds for $S = 1/2$ Heisenberg J_1-J_2 chain magnets. In this situation, findings obtained in a comprehensive study on a new candidate compound may lead to a major breakthrough.

*fujihala@post.j-parc.jp

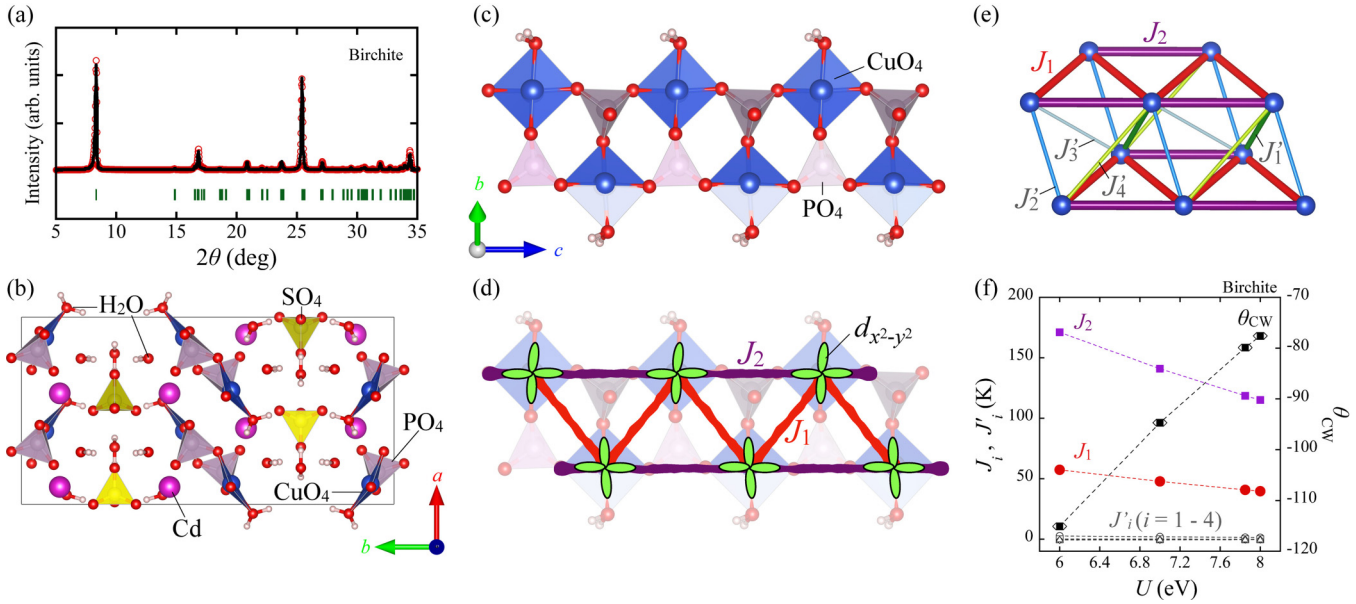

FIG. 1. (a) XRD intensity pattern (open red circles) observed for $Cd_2Cu_2(PO_4)_2SO_4 \cdot 5H_2O$ at room temperature. The simulated XRD profile using the computer program RIETAN-FP is shown by a black solid line. The green vertical bars indicate the position of Bragg reflection peaks. (b) Crystal structure of $Cd_2Cu_2(PO_4)_2SO_4 \cdot 5H_2O$. The atomic hydrogen positions are optimized by GGA calculations. (c) An isolated segment of the J_1-J_2 chain. (d) Arrangement of the Cu^{2+} orbitals in a chain. J_1 and J_2 are intrachain interactions. (e) Exchange network between Cu^{2+} sites in a $1 \times 1 \times 2$ supercell. (f) Exchange interactions of $Cd_2Cu_2(PO_4)_2SO_4 \cdot 5H_2O$ extracted by DFT energy mapping. Couplings are shown as a function of local Coulomb repulsion U, while Hund's rule coupling was fixed to $J_H = 1$ eV.

Here we report the magnetic behavior of birchite $Cd_2Cu_2(PO_4)_2SO_4 \cdot 5H_2O$, which we successfully synthesized as a single-phase polycrystalline sample. In addition, we performed density functional theory (DFT) calculations and finite-temperature Lanczos (FTL) calculations [36] of the magnetic susceptibility to determine and evaluate the magnetic Hamiltonian of birchite.

II. EXPERIMENTAL AND COMPUTATIONAL DETAILS

The synthesis of $Cd_2Cu_2(PO_4)_2SO_4 \cdot 5H_2O$ has been designed after the identification of the natural mineral birchite. Single-phase polycrystalline $Cd_2Cu_2(PO_4)_2SO_4 \cdot 5H_2O$ was finally successfully synthesized by using a hydrothermal reaction. Aqueous solutions of 2 M $CuSO_4$ and 2 M $CdSO_4$ and 10 M H_3PO_4 were mixed in a PTFE liner and sealed in a steel autoclave. The autoclave was heated to 150 °C for several hours in a convection oven and cooled to room temperature by turning off the oven. Then the product was thoroughly washed with pure water. The crystal structure of the obtained polycrystalline sample was examined by x-ray diffraction (XRD, Rigaku Ultima IV). Then the XRD profile was simulated with the Rietveld refinement program RIETAN-FP [37]. Magnetic susceptibility measurements were performed using a commercial superconducting quantum interference device magnetometer (MPMS; Quantum Design). Furthermore, high-field magnetization measurements up to 60 T were carried out using an induction method in a pulsed magnetic field. The specific heat was measured between 0.4 and 300 K using a physical property measurement system (PPMS; Quantum Design). Zero-field (ZF) and longitudinal-field (LF) μSR experiments are performed using the spin-polarized pulsed surface-muon (μ^+) beam at the S1 beam line of the Materials and Life Science Experimental Facility (MLF) of the Japan Proton Accelerator Research Complex (J-PARC). We perform all electron density functional theory calculations using the full-potential local-orbital (FPLO) code [38]. We use the generalized gradient approximation (GGA) exchange-correlation functional [39]. Furthermore, we deal with the strong electronic correlations in the Cu^{2+} $3d$ orbitals with a GGA + U correction [40]. While the Hund's rule coupling J_H is kept fixed at 1 eV in accordance with earlier studies, we vary the on-site Coulomb interaction U [41,42]. For the GGA + U calculations, an atomic limit double-counting correction was used.

III. RESULTS AND DISCUSSION

The natural birchite crystallizes in the orthorhombic system with the space group *Pnma* and the parameters $a = 10.489(6)$ Å, $b = 20.901(7)$ Å, and $c = 6.155(5)$ Å, with $Z = 4$ [43]. As shown in Fig. 1(a), the powder XRD pattern of synthetic $Cd_2Cu_2(PO_4)_2SO_4 \cdot 5H_2O$ is consistent with peak positions calculated using these parameters. The crystal structure of $Cd_2Cu_2(PO_4)_2SO_4 \cdot 5H_2O$ is shown in Fig. 1(b). The PO_4 tetrahedra corner share with three adjacent CuO_4 plaquettes, forming a J_1-J_2 (zigzag) chain along the c axis [Fig. 1(c)]. The zigzag chain along the c axis is formed by two different exchange interactions mediated by the Cu-O-P-O-Cu path. By analogy with the J_1-J_2 model, we labeled the magnetic interaction corresponding to the shorter distance as J_1 and the longer distance as J_2 [Fig. 1(d)]. The orbital arrangements can be reasonably deduced from the positions of oxygen around the Cu^{2+} ion. In crystal field theory, the five $3d$ orbitals in

TABLE I. Exchange couplings of $Cd_2Cu_2(PO_4)_2SO_4 \cdot 5H_2O$, calculated within GGA + U at $J_H = 1$ eV and $1 \times 1 \times 2$ k points in a supercell containing 10 Cu^{2+} sites. Paths are identified by Cu-Cu distance (last row). Note that J_1 and J_2 correspond to second and fifth shortest Cu-Cu distances. The Curie-Weiss temperature was calculated using Eq. (1). J'_5, J'_{10}, J'_{12}, and J'_{14} couplings connecting the Cu chains along crystallographic b direction are negligibly small and are not shown in Fig 1.

U (eV)	J_1 (K)	J_2 (K)	J'_1 (K)	J'_2 (K)	J'_3 (K)	J'_4 (K)	J'_5 (K)	J'_{10} (K)	J'_{12} (K)	J'_{14} (K)	θ_{CW} (K)
6	57.4(4)	171.7(1.0)	2.7(1.0)	−0.1(1.0)	−0.7(1.9)	0.2(1.1)	−0.2(4)	−0.0(5)	0.0(2)	0.0(5)	−115.1
7	47.8(3)	141.0(7)	2.0(7)	−0.1(7)	−0.6(1.3)	0.1(7)	0.1(3)	0.0(3)	0.0(2)	0.0(3)	−94.7
7.85	40.8(3)	118.6(7)	1.5(6)	−0.1(6)	−0.4(1.2)	0.0(7)	−0.1(3)	0.0(3)	0.0(2)	0.0(3)	−79.9
8	39.7(2)	115.1(5)	1.4(5)	−0.1(5)	−0.4(9)	0.0(5)	−0.1(2)	0.0(3)	0.0(1)	0.0(3)	−77.6
d_{Cu-Cu} (Å)	5.02716	6.164	3.79212	5.47541	5.8331	6.95199	7.803	9.53241	9.94393	10.4507	

a square-planar field produced by four surrounding anions split into e_g, a_{1g}, b_{2g}, and b_{1g} orbitals with different energies. Since the b_{1g} orbital possesses the highest energy, all the Cu^{2+} ions have their unpaired electrons in the $d_{x^2-y^2}$ orbital. Double chains of CuO_4 plaquettes are stringed up along the c axis. The strong exchange interactions J_1 and J_2 are mediated by PO_4^{3-} ions. In the a direction, these double chains are separated by Cd^{2+} ions, and as the $d_{x^2-y^2}$ orbitals are parallel to each other, interchain interactions along a should be weak [see Fig. 1(b)]. Along b, the long interchain separation filled with H_2O molecules also leads to negligible exchange.

The magnitude of the inter- and intrachain interactions of $Cd_2Cu_2(PO_4)_2SO_4 \cdot 5H_2O$ was evaluated using energy mapping [44–46]. For this purpose, a $1 \times 1 \times 2$ supercell with 16 independent Cu^{2+} sites was created. As the atomic positions of hydrogen were not determined experimentally, they were optimized by GGA calculations. This allows us to estimate intrachain interactions J_1 and J_2 and interchain interactions J'_1 to J'_5, J'_{10}, J'_{12}, and J'_{14}. J_1, J_2 and J'_1 to J'_4 correspond to Cu-Cu distances between 3.79 Å and 6.96 Å, connecting the Cu^{2+} ions into a buckled two-dimensional lattice; these six different exchange paths are shown in Fig. 1(e). The energy mapping for three values of the on-site interaction U is shown in Fig. 1(f). See Table I with all the determined couplings. The Curie-Weiss temperature estimates are obtained from the standard expression [47]

$$\theta_{CW} = -\frac{2}{3}S(S+1)\left(J_1 + J_2 + \frac{J'_1}{2} + J'_2 + \frac{J'_3}{2} + J'_4 + \frac{J'_5}{2} + J'_{10} + J'_{12} + J'_{14}\right), \quad (2)$$

where $S = 1/2$ and exchange couplings are weighted with coordination numbers. We compare the exchange interactions obtained for $U = 6$, 7, and 8 eV. Note that the value of the on-site Coulomb repulsion U can be expected to be around $U = 8$ eV, which has been found to correctly describe many magnetic materials based on Cu^{2+} [48,49]. The interchain interactions are two orders of magnitude smaller than J_2, which is consistent with the crystal structure features. In light of this result, $Cd_2Cu_2(PO_4)_2SO_4 \cdot 5H_2O$ can be regarded as a J_1-J_2 antiferromagnet ($J_1 > 0$ and $J_2 > 0$). One of the prominent and important features of this compound is that the magnitude of J_2 is two to three times larger than that of J_1. There are a few J_1-J_2 known antiferromagnets, such as $CuGeO_3$ [10,11], $KTi(SO_4)_2H_2O$ [12,13], and $(N_2H_5)CuCl_3$ [14–16], in which the J_2/J_1 ratio is reported to be about 0.35, 0.29, and 4, respectively. In $KTi(SO_4)_2H_2O$ and $(N_2H_5)CuCl_3$, a small spin gap $\Delta < J_1/20$ is expected to exist [50]. The fact that the small gap has not been observed may be due to the required cooling of the sample down to the mK region. In contrast, for $Cd_2Cu_2(PO_4)_2SO_4 \cdot 5H_2O$, the presence of a spin gap will be determined by experiments at relatively accessible temperatures, i.e., above 0.3 K.

Figures 2(a) and 2(b) present the magnetic susceptibility and the magnetization curve of $Cd_2Cu_2(PO_4)_2SO_4 \cdot 5H_2O$. The intrinsic susceptibility $\chi_{bulk}(T)$ is obtained by subtracting Pascal's diamagnetic contribution $\chi_{dia.}$ [51] and Curie tail contribution $\chi_{free} = n_{free}C/T$ from the experimental data $\chi_{obs.}$. Here, C is the Curie constant for spin-1/2 with the fixed g factor as $g = 2.0$, namely, χ_{free} is assumed to be a component due to paramagnetic impurities or unpaired spins on the surface of powder particles. As compared with the susceptibility at low temperatures, $T < 5$ K in Fig. 2(a), we determine the parameter as $n_{free} = 0.007$. The intrinsic magnetization $M_{bulk}(H)$ is also obtained by subtracting the contribution of free spins from the experimental data by using the following equation: $n_{free}gS\mu_B[2\coth(gS\mu_BH/k_BT) - \coth(gS\mu_BH/2k_BT)]$. As shown in the inset in Fig. 2(b), the behavior of $M_{bulk}(H)$ with $n_{free} = 0.007$ is consistent with that of one-dimensional antiferromagnets. Therefore, we expect about 0.7% of all Cu^{2+} ions in our sample to be free spins. From $1/\chi_{bulk}(T)$ with the Curie-Weiss law $C/(T - \theta_{CW})$, between 250 and 300 K, we estimated the Curie constant and Curie-Weiss temperature to be $C = 0.46(1)$/emu/K/mol-Cu and $\theta_{CW} = -79.9(9)$ K, respectively. The C corresponds to an effective moment of 1.93(4) μ_B and it is slightly higher than the spin-only value (= 1.73 μ_B). We use the experimentally determined Curie-Weiss temperature $\theta_{CW} = -79.9$ K to select the relevant on-site interaction as $U = 7.85$ eV; this yields the set of intrachain interactions $J_1 = 40.8$ K and $J_2 = 118.6$ K. However, the magnetic susceptibility calculated using these values is not in good agreement with the $\chi_{bulk}(T)$. The reason for this disagreement may be due to uncertainty in the determination of the θ_{CW}. The Curie-Weiss law holds in the paramagnetic region above the magnetic transition temperature. The θ_{CW} in Eq. (2) is a result in the high-temperature limit. In the case of low-dimensional quantum spin systems, it is known that the θ_{CW} is not accurate unless the fitting of the magnetic susceptibility is done at sufficiently high temperatures compared to the exchange interactions [52]. In our experiments, the θ_{CW} is determined from a fitting of the

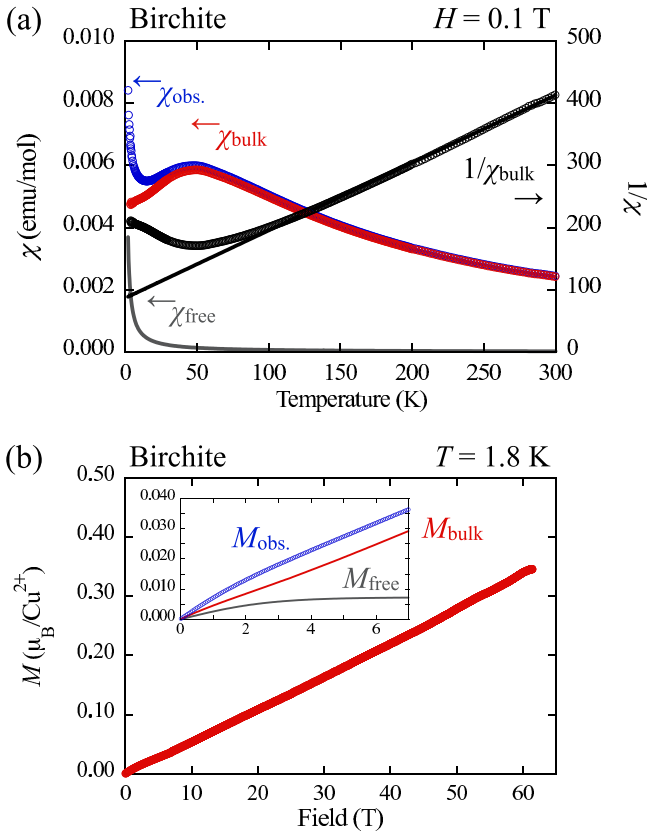

FIG. 2. (a) Temperature dependence of the intrinsic magnetic susceptibility χ_{bulk} (red circles) and the inverse susceptibility $1/\chi_{bulk}$ (black circles) of $Cd_2Cu_2(PO_4)_2SO_4 \cdot 5H_2O$ measured at 0.1 T. The χ_{bulk} is obtained by subtracting Pascal's diamagnetic contribution $\chi_{dia.}$ and an estimated contribution of free spins χ_{free} (gray solid line) from the experimental data $\chi_{obs.}$. The solid and broken green lines denote the fitting curves by the Curie-Weiss law. (b) High-field magnetization at 1.8 K. Inset shows the magnetization measured using MPMS at 1.8 K. The observed data $M_{obs.}$ (open blue circles) are broken down into two components: M_{bulk} (red solid line) and M_{free} (gray solid line). The gray line is the Brillouin function for $g = 2$ and 0.7% of free $S = 1/2$ spins.

magnetic susceptibility at about $T = 250$ to 300 K, which is not a high enough temperature. It is therefore difficult to determine an accurate θ_{CW} value in $Cd_2Cu_2(PO_4)_2SO_4 \cdot 5H_2O$.

In order to further validate the magnitude of the intrachain interactions, we calculated the magnetic susceptibility by the exact diagonalization (ED) and FTL method. As reported in Ref. [13], such numerical methods can reproduce the experimental data with two different results, in the case of $J_2/J_1 > 1$ and $J_2/J_1 < 1$, and cannot distinguish between them. Thus, the ED and FTL calculations were performed by imposing the condition revealed by the energy mapping calculation that $J_2/J_1 > 1$. We succeeded in reproducing the magnetic susceptibility of $Cd_2Cu_2(PO_4)_2SO_4 \cdot 5H_2O$ with the J_1-J_2 model with $J_1 = 27.48$ K, $J_2 = 78.50$ K, and $g = 2.145$, as shown in Fig. 3. The ratio of $J_2/J_1 \simeq 2.86$ is consistent with that obtained by the DFT calculations with $U = 8$ eV. As shown in Fig. 2(b), the high-field magnetization increases linearly even around one-third of the saturation magnetization, indicating that there is no plateau. This experimental result is consistent

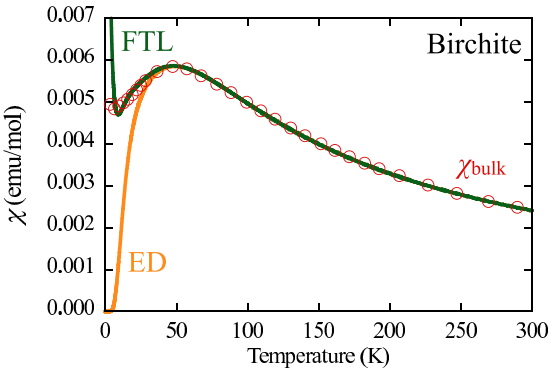

FIG. 3. Temperature dependence of the magnetic susceptibility χ_{bulk} (open red circles; only 30% of all data points are displayed) of $Cd_2Cu_2(PO_4)_2SO_4 \cdot 5H_2O$ and the fitted calculation data obtained by the FTL method for a 35-site cluster (green line) and ED method for an 18-site cluster (orange line).

with the theoretical result in Ref. [3] that the magnetization plateau appears when the ratio is $0.56 \leqq J_2/J_1 \leqq 1.25$.

Muons, having a large gyromagnetic ratio, are a sensitive microscopic probe for magnetic order and spin fluctuations. Figure 4(a) shows the asymmetry spectra measured at 153 and 2.3 K under zero field (ZF) and low field (LF) of 20 and

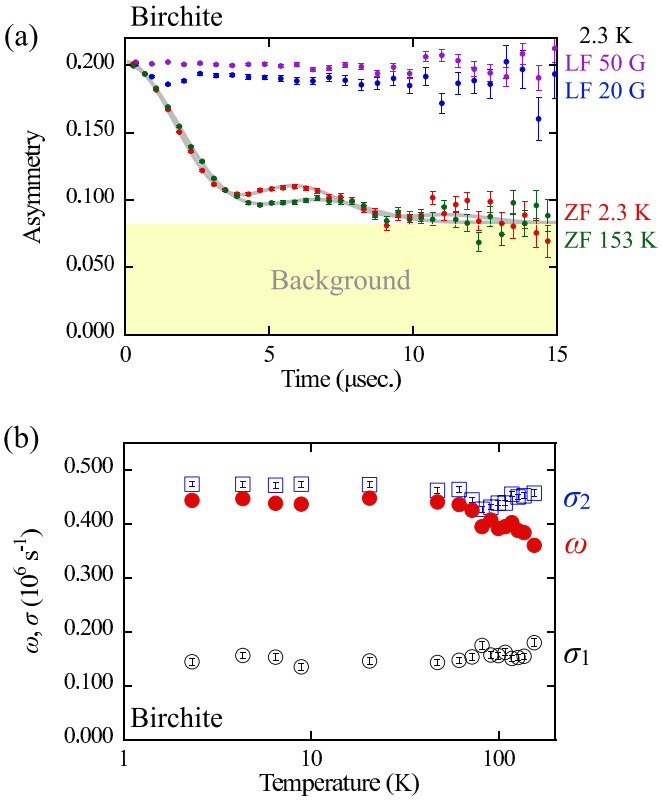

FIG. 4. (a) ZF-μSR spectra at representative temperatures and LF-μSR spectra measured at 2.3 K under 20 and 50 G. The thick lines behind the data points are the fitted curves (see text for details). (b) Temperature dependence of dipolar interaction angular frequency ω (filled red circles), relaxation rate σ_1 of the H-μ-H signal (open black circles), and relaxation rate σ_2.

50 G. At 2.3 K, well below the broad peak in the magnetic susceptibility, the local field can be fully decoupled even at the fields of 50 G. Therefore, the oscillation is due to the nuclear magnetism. The positive muons are known to stop in the vicinity of the anion and H_2O molecules in hydrate crystals, and H_2O and μ^+ form H-μ^+-H units [53]. All ZF-μSR spectra can be fitted by a combination of two signals: one part containing a relaxing precession signal due to the formation of H-μ^+-H units and a second part with a Gaussian relaxation signal,

$$A_0 P_{\mathrm{ZF}}(t) = A_1 P_{\mathrm{H}\mu\mathrm{H}}(t) \exp\left(-\frac{\sigma_1^2 t^2}{2}\right) + A_2 \exp\left(-\frac{\sigma_2^2 t^2}{2}\right) + A_{\mathrm{BG}}, \quad (3)$$

where A_0 is the initial asymmetry, and A_1 and A_2 are the intrinsic asymmetries $A_1 = 0.054$ and $A_2 = 0.067$. A_1 represents the fraction of muons that stops near H_2O and A_2 represents the fraction of muons that stops at different muon sites. A_{BG} is the constant background $A_{\mathrm{BG}} = 0.082$. σ_1 and σ_2 are the Gaussian relaxation rates, and $P_{\mathrm{H}\mu\mathrm{H}}(t)$ is the muon spin depolarization function caused by forming H-μ^+-H units. The $P_{\mathrm{H}\mu\mathrm{H}}(t)$ signal is represented by [53]

$$P_{\mathrm{H}\mu\mathrm{H}}(t) = \frac{1}{2} + \frac{1}{6}\cos\left(\sqrt{3}\omega t\right) + \frac{1+\frac{1}{\sqrt{3}}}{6}\cos\left(\frac{3+\sqrt{3}}{2}\omega t\right) + \frac{1-\frac{1}{\sqrt{3}}}{6}\cos\left(\frac{3-\sqrt{3}}{2}\omega t\right), \quad (4)$$

where ω is the muon precession angular frequency due to the nuclear dipole field of the proton in the H-μ^+-H bond. The first term in Eq. (3), which multiplies $P_{\mathrm{H}\mu\mathrm{H}}(t)$ by a Gaussian function, is a phenomenological approach that considers the effects of next-nearest-neighbor hydrogen ions, etc. The distance d between μ^+ and the nucleus can be calculated by

$$\omega = \mu_0 \hbar \frac{\gamma_\mu \gamma_N}{4\pi d^3}, \quad (5)$$

where μ_0 is the permeability of vacuum, $\hbar$ is the reduced Planck constant, γ_μ is the gyromagnetic ratio of the positive muon, and γ_N is the nuclear gyromagnetic ratio of ^{1}H.

At high temperatures, the H-μ^+-H bond should not be stable due to thermal vibrations of H_2O [54,55]. In fact, as shown in Fig. 4, the μSR parameters show a temperature dependence only at high temperatures. Thus, we determined the magnetic field distributions and d of $Cd_2Cu_2(PO_4)_2SO_4 \cdot 5H_2O$ using data below 50 K. The magnetic field distribution is $\sigma_1/\gamma_\mu = 1.72(8)$ G, which is typical for forming H-μ^+-H. The $\sigma_2/\gamma_\mu = 5.53(5)$ G is also typical for a nuclear dipole field. The d is estimated as 1.75(2) Å, which is consistent with the reported value of $[Ca_{0.85}OH]_{1.16}[CoO_2]$ and water-intercalated sodium cobalt dioxides [56,57]. μSR measurements provide evidence for the absence of spin ordering/freezing at least above 2.3 K in $Cd_2Cu_2(PO_4)_2SO_4 \cdot 5H_2O$.

The existence of the spin gap in $Cd_2Cu_2(PO_4)_2SO_4 \cdot 5H_2O$ is suggested by specific heat measurements. As shown in Fig. 5(a), the curve does not show a pronounced λ-type peak, indicating that a second-order phase transition does not occur down to at least 0.4 K. A Schottky-like peak is observed at around $T \simeq 1$ K. In the present case, we also could not get a precise estimation of the lattice contribution. From the temperature dependence of C, between 12 and 15 K, we roughly estimate the lattice specific heat component to be 0.004 T^3. The C/T peak originating from the Schottky-like anomaly is observed at around $T \simeq 2$ K, as shown in Fig. 5(b). The Schottky anomaly in the specific heat takes the form $C_{\mathrm{Sch.}} = R(\Delta/T)^2 \exp(\Delta/T)/[1+\exp(\Delta/T)]^2$, where R is the gas constant and Δ is the energy level expressed in Kelvin. Assuming that this magnetic component comes from free spins, it can be described by $n_{\mathrm{free}}\, C_{\mathrm{Sch.}}/T$. As shown in Fig. 5(b), the peak positions of $n_{\mathrm{free}}\, C_{\mathrm{Sch.}}/T$ with $n_{\mathrm{free}} = 0.007$ and $\Delta = 6$ K and experimental data are roughly consistent;

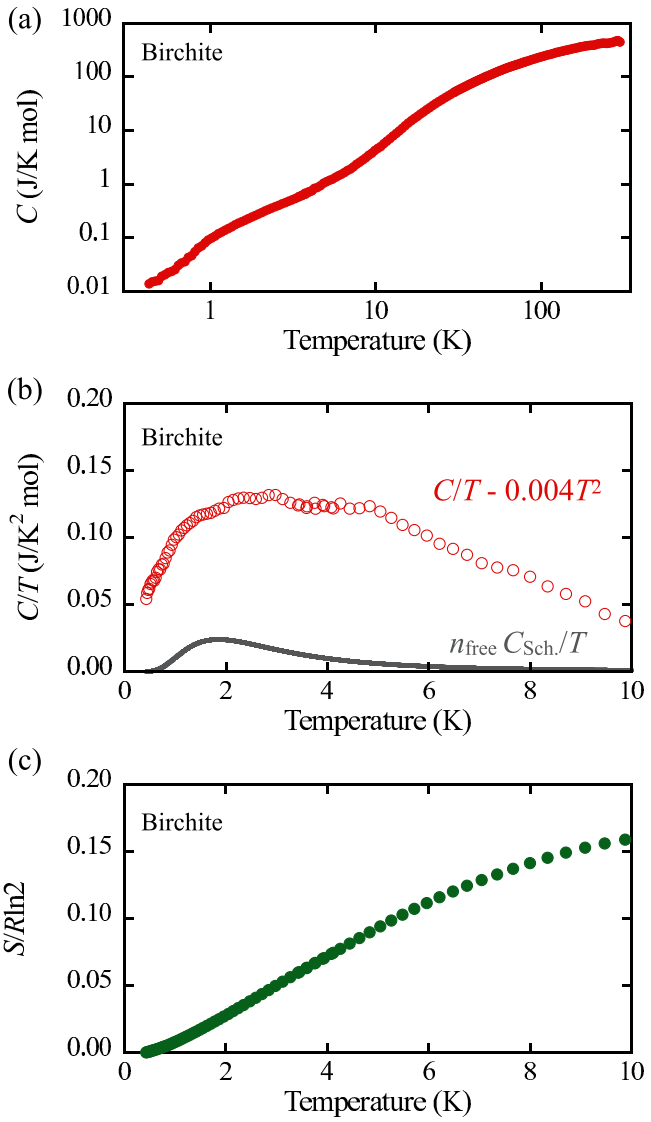

FIG. 5. (a) The temperature dependence of the total specific heat (filled red circles) for zero magnetic field. (b) The extracted magnetic specific heat divided by temperature (open red circles). The magnetic specific heat is the assumed lattice specific heat component (0.004 T^3) subtracted from the total specific heat. The gray solid line is the calculated specific heat of the free spins, as discussed in the text. (c) Temperature dependence of the estimated magnetic entropy.

however, the magnitude is not reproduced at all. Therefore, the anomaly is due to intrinsic magnetic behavior rather than free spins. On the other hand, this anomaly cannot be fitted by a simple two-level Schottky model $C_{\mathrm{Sch.}}/T$. Figure 5(c) shows the temperature dependence of the released magnetic entropy associated with the Schottky-like anomaly, which is obtained by the integration of C/T. The released magnetic entropy at 10 K is only 16% of the expected total entropy. Further studies are necessary to deepen the understanding of this anomaly, including precise estimation of the lattice component and specific heat measurement in a magnetic field. The peak seems to develop from higher temperatures than 2.3 K. On the other hand, the signal due to slowing down of the electron spin magnetic moment fluctuations is not observed in the μSR spectra. We conclude that the Cu^{2+} spins form singlet pairs and the magnetic moment disappears below 2 K.

IV. CONCLUSIONS

In summary, we presented evidence that birchite $Cd_2Cu_2(PO_4)_2SO_4 \cdot 5H_2O$ is a very good realization of an $S = 1/2$ Heisenberg J_1-J_2 chain antiferromagnet. Our calculations reveal that J_1 and J_2 are antiferromagnetic and their magnitude is about 100 times larger than the interchain interactions. The magnitude of J_2 is two to three times larger than that of J_1. Our experimental investigation provides evidence for the absence of magnetic ordering/freezing in $Cd_2Cu_2(PO_4)_2SO_4 \cdot 5H_2O$ down to 0.4 K. Specific heat measurements suggest the existence of a spin gap. The Schottky-like peak is observed at 1 K, which is about 3.6% of J_1, consistent with previously reported density matrix renormalization group calculations [50]. We suggest that $Cd_2Cu_2(PO_4)_2SO_4 \cdot 5H_2O$ is a notable compound among the $S = 1/2$ Heisenberg J_1-J_2 chain antiferromagnets as it probably has an experimentally observable spin gap. Further experimental studies are needed to confirm the presence or absence of a spin gap.

ACKNOWLEDGMENTS

The μSR experiment was performed at the MLF of J-PARC under a user program (Proposal No. 2020A0066). This study is supported by the Grant-in-Aid for Scientific Research (Grants No. 21K03453 and No. 17K1434) from MEXT, Japan.

APPENDIX A: DETAILS OF ENERGY MAPPING

The energy mapping method uses DFT + U total energies to determine the relevant Heisenberg Hamiltonian parameters for a material. For this purpose, a supercell is constructed which allows resolution of a sufficient number of exchange couplings. In the case of birchite $Cd_2Cu_2(PO_4)_2SO_4 \cdot 5H_2O$, determination of J_2 requires doubling of the unit cell along the c direction. The $1 \times 1 \times 2$ supercell in $P1$ symmetry with 16 independent Cu sites allows for 65 536 spin configurations, 1691 of which have distinct energy expressions. The system of equations allows us to extract 10 exchange interactions, and among them the first seven nearest-neighbor Cu-Cu exchanges. It is an important ingredient of the energy mapping method to calculate many more than the minimal 11 DFT + U total energies and to extract the 10 couplings by a least-squares fit (rather than solving the minimal set of linear equations). Figure 6 shows the quality of fit of 28 DFT + U energies. The excellent fit indicates that the method works very well for birchite, which has an average energy gap of $E_g = 2.4$ eV for all spin configurations at $U = 8$ eV. We have performed structural relaxation using GGA + U with $U = 7.85$ eV and found that the experimental structure changes only minimally (not shown here). This indicates consistency between the crystal structure and the magnetic Hamiltonian that we determined.

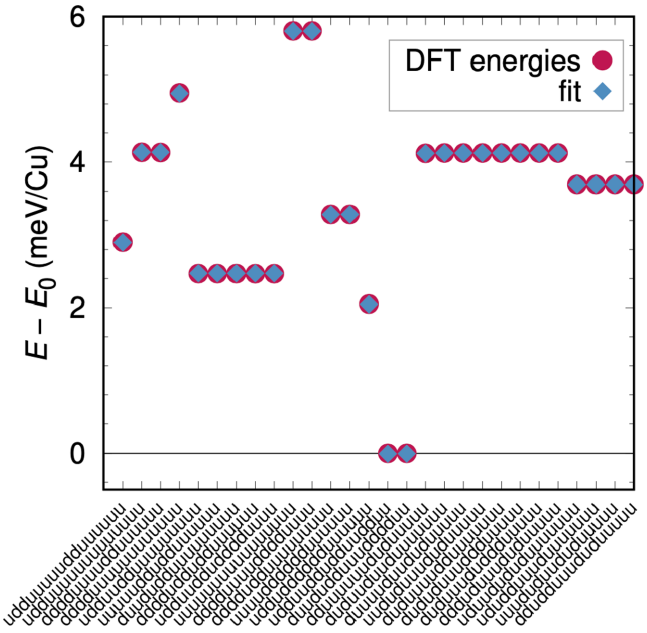

FIG. 6. Total DFT energies for different spin configurations of a $1 \times 1 \times 2$ supercell of $Cd_2Cu_2(PO_4)_2SO_4 \cdot 5H_2O$ calculated at $U = 8$ eV and $J_H = 1$ eV (circles), shown together with the fit to the Heisenberg Hamiltonian (diamonds). The fit is perfect.

[1] C. K. Majumdar and D. K. Ghosh, On Next-Nearest-Neighbor Interaction in Linear Chain. I, J. Math. Phys. **10**, 1388 (1969).
[2] *Frustrated Spin Systems*, edited by H. T. Diep (World Scientific, Singapore, 2005).
[3] K. Okamoto and K. Nomura, Fluid-dimer critical point in $S = 1/2$ antiferromagnetic Heisenberg chain with next nearest neighbor interactions, Phys. Lett. A **169**, 433 (1992).
[4] K. Okunishi and T. Tonegawa, Magnetic phase diagram of the $S = 1/2$ antiferromagnetic zigzag spin chain in the strongly frustrated region: Cusp and plateau, J. Phys. Soc. Jpn. **72**, 479 (2003).
[5] K. Okunishi, On calculation of vector spin chirality for zigzag spin chains, J. Phys. Soc. Jpn. **77**, 114004 (2008).

[6] J. Sirker, V. Y. Krivnov, D. V. Dmitriev, A. Herzog, O. Janson, S. Nishimoto, S.-L. Drechsler, and J. Richter, J_1-J_2 Heisenberg model at and close to its $z = 4$ quantum critical point, Phys. Rev. B **84**, 144403 (2011).

[7] H. P. Bader and R. Schilling, Conditions for a ferromagnetic ground state of Heisenberg Hamiltonians, Phys. Rev. B **19**, 3556 (1979).

[8] A. A. Nersesyan, A. O. Gogolin, and F. H. L. Essler, Incommensurate Spin Correlations in Spin-1/2 Frustrated Two-Leg Heisenberg Ladders, Phys. Rev. Lett. **81**, 910 (1998).

[9] T. Hikihara, L. Kecke, T. Momoi, and A. Furusaki, Vector chiral and multipolar orders in the spin-$\frac{1}{2}$ frustrated ferromagnetic chain in magnetic field, Phys. Rev. B **78**, 144404 (2008).

[10] J. Riera and A. Dobry, Magnetic susceptibility in the spin-Peierls system $CuGeO_3$, Phys. Rev. B **51**, 16098 (1995).

[11] M. Hase, I. Terasaki, and K. Uchinokura, Observation of the Spin-Peierls Transition in Linear Cu^{2+} (Spin-1/2) Chains in an Inorganic Compound $CuGeO_3$, Phys. Rev. Lett. **70**, 3651 (1993).

[12] G. J. Nilsen, H. M. Rønnow, A. M. Läuchli, F. P. A. Fabbiani, J. Sanchez-Benitez, K. V. Kamenev, and A. Harrison, A new realisation of the $S = 1/2$ frustrated chain antiferromagnet, Chem. Mater. **20**, 8 (2008).

[13] D. Kasinathan, K. Koepernik, O. Janson, G. J. Nilsen, J. O. Piatek, H. M. Rønnow, and H. Rosner, Electronic structure of $KTi(SO_4)_2 \cdot H_2O$: An $S = 1/2$ frustrated chain antiferromagnet, Phys. Rev. B **88**, 224410 (2013).

[14] D. B. Brown, J. A. Donner, J. W. Hall, S. R. Wilson, R. B. Wilson, D. J. Hodgson, and W. E. Hatfield, Interaction of hydrazine with copper(II) chloride in acidic solutions. Formation, spectral and magnetic properties, and structures of copper(II), copper(I), and mixed-valence species, Inorg. Chem. **18**, 2635 (1979).

[15] M. Hagiwara, Y. Narumi, K. Kindo, N. Maeshima, K. Okunishi, T. Sakai, and M. Takahashi, High-field magnetization of an $S = 1/2$ zigzag chain compound $(N_2H_5)CuCl_3$, Phys. B: Condens. Matter **294-295**, 83 (2001).

[16] N. Maeshima, M. Hagiwara, Y. Narumi, K. Kindo, T. C. Kobayashi, and K. Okunishi, Magnetic properties of a $S = 1/2$ zigzag spin chain compound $(N_2H_5)CuCl_3$, J. Phys.: Condens. Matter **15**, 3607 (2003).

[17] L. E. Svistov, T. Fujita, H. Yamaguchi, S. Kimura, K. Omura, A. Prokofiev, A. I. Smirnov, Z. Honda, and M. Hagiwara, New high magnetic field phase of the frustrated $S = 1/2$ chain compound $LiCuVO_4$, JETP Lett. **93**, 21 (2011).

[18] T. Masuda, M. Hagihala, Y. Kondoh, K. Kaneko, and N. Metoki, Spin density wave in insulating ferromagnetic frustrated chain $LiCuVO_4$, J. Phys. Soc. Jpn. **80**, 113705 (2011).

[19] M. Mourigal, M. Enderle, B. Fåk, R. K. Kremer, J. M. Law, A. Schneidewind, A. Hiess, and A. Prokofiev, Evidence of a Bond-Nematic Phase in $LiCuVO_4$, Phys. Rev. Lett. **109**, 027203 (2012).

[20] K. Nawa, M. Takigawa, M. Yoshida, and K. Yoshimura, Anisotropic Spin Fluctuations in the Quasi One-Dimensional Frustrated Magnet $LiCuVO_4$, J. Phys. Soc. Jpn. **82**, 094709 (2013).

[21] N. Büttgen, K. Nawa, T. Fujita, M. Hagiwara, P. Kuhns, A. Prokofiev, A. P. Reyes, L. E. Svistov, K. Yoshimura, and M. Takigawa, Search for a spin-nematic phase in the quasi-one-dimensional frustrated magnet $LiCuVO_4$, Phys. Rev. B **90**, 134401 (2014).

[22] A. Orlova, E. L. Green, J. M. Law, D. I. Gorbunov, G. Chanda, S. Krämer, M. Horvatić, R. K. Kremer, J. Wosnitza, and G. L. J. A. Rikken, Nuclear Magnetic Resonance Signature of the Spin-Nematic Phase in $LiCuVO_4$ at High Magnetic Fields, Phys. Rev. Lett. **118**, 247201 (2017).

[23] M. Gen, T. Nomura, D. I. Gorbunov, S. Yasin, P. T. Cong, C. Dong, Y. Kohama, E. L. Green, J. M. Law, M. S. Henriques *et al.*, Magnetocaloric effect and spin-strain coupling in the spin-nematic state of $LiCuVO_4$, Phys. Rev. Res. **1**, 033065 (2019).

[24] B. Willenberg, M. Schäpers, K. C. Rule, S. Süllow, M. Reehuis, H. Ryll, B. Klemke, K. Kiefer, W. Schottenhamel, B. Büchner *et al.*, Magnetic Frustration in a Quantum Spin Chain: The Case of Linarite $PbCuSO_4(OH)_2$, Phys. Rev. Lett. **108**, 117202 (2012).

[25] M. Schäpers, A. U. B. Wolter, S.-L. Drechsler, S. Nishimoto, K.-H. Müller, M. Abdel-Hafiez, W. Schottenhamel, B. Büchner, J. Richter, B. Ouladdiaf *et al.*, Thermodynamic properties of the anisotropic frustrated spin-chain compound linarite $PbCuSO_4(OH)_2$, Phys. Rev. B **88**, 184410 (2013).

[26] B. Willenberg, M. Schäpers, A. U. B. Wolter, S.-L. Drechsler, M. Reehuis, J.-U. Hoffmann, B. Büchner, A. J. Studer, K. C. Rule, B. Ouladdiaf *et al.*, Complex Field-Induced States in Linarite $PbCuSO_4(OH)_2$ with a Variety of High-Order Exotic Spin-Density Wave States, Phys. Rev. Lett. **116**, 047202 (2016).

[27] Y. Feng, K. Y. Povarov, and A. Zheludev, Magnetic phase diagram of the strongly frustrated quantum spin chain system $PbCuSO_4(OH)_2$ in tilted magnetic fields, Phys. Rev. B **98**, 054419 (2018).

[28] L. Heinze, G. Bastien, B. Ryll, J.-U. Hoffmann, M. Reehuis, B. Ouladdiaf, F. Bert, E. Kermarrec, P. Mendels, S. Nishimoto *et al.*, Magnetic phase diagram of the frustrated spin chain compound linarite $PbCuSO_4(OH)_2$ as seen by neutron diffraction and ^{1}H-NMR, Phys. Rev. B **99**, 094436 (2019).

[29] K. Nawa, Y. Okamoto, A. Matsuo, K. Kindo, Y. Kitahara, S. Yoshida, S. Ikeda, S. Hara, T. Sakurai, S. Okubo, H. Ohta, and Z. Hiroi, $NaCuMoO_4(OH)$ as a candidate frustrated J_1-J_2 chain quantum magnet, J. Phys. Soc. Jpn. **83**, 103702 (2014).

[30] K. Nawa, M. Yoshida, M. Takigawa, Y. Okamoto, and Z. Hiroi, Collinear spin density wave order and anisotropic spin fluctuations in the frustrated J_1-J_2 chain magnet $NaCuMoO_4(OH)$, Phys. Rev. B **96**, 174433 (2017).

[31] S. Asai, T. Oyama, K. Nawa, A. Nakao, K. Munakata, K. Kuwahara, M. Hagihala, S. Itoh, Z. Hiroi, and T. Masuda, Helical and collinear spin density wave order in the $S = \frac{1}{2}$ one-dimensional frustrated chain compound $NaCuMoO_4(OH)$ investigated by neutron scattering, Phys. Rev. B **101**, 144437 (2020).

[32] M. Pregelj, A. Zorko, O. Zaharko, H. Nojiri, H. Berger, L. C. Chapon, and D. Arčon, Spin-stripe phase in a frustrated zigzag spin-1/2 chain, Nat. Commun. **6**, 7255 (2015).

[33] F. Weickert, N. Harrison, B. L. Scott, M. Jaime, A. Leitmäe, I. Heinmaa, R. Stern, O. Janson, H. Berger, H. Rosner *et al.*, Magnetic anisotropy in the frustrated spin-chain compound β-$TeVO_4$, Phys. Rev. B **94**, 064403 (2016).

[34] M. Pregelj, A. Zorko, M. Klanjšek, O. Zaharko, J. S. White, O. Prokhnenko, M. Bartkowiak, H. Nojiri, H. Berger, and D. Arčon, Magnetic ground state of the frustrated spin-1/2 chain

compound β-$TeVO_4$ at high magnetic fields, Phys. Rev. B **100**, 094433 (2019).

[35] S. Nishimoto, S.-L. Drechsler, R. O. Kuzian, J. van den Brink, J. Richter, W. E. A. Lorenz, Y. Skourski, R. Klingeler, and B. Büchner, Saturation Field of Frustrated Chain Cuprates: Broad Regions of Predominant Interchain Coupling, Phys. Rev. Lett. **107**, 097201 (2011).

[36] J. Jaklič and P. Prelovšek, Lanczos method for the calculation of finite-temperature quantities in correlated systems, Phys. Rev. B **49**, 5065 (1994).

[37] F. Izumi and K. Momma, Three-dimensional visualization in powder diffraction, Solid State Phenom. **130**, 15 (2007).

[38] K. Koepernik and H. Eschrig, Full-potential nonorthogonal local-orbital minimum-basis band-structure scheme, Phys. Rev. B **59**, 1743 (1999).

[39] J. P. Perdew, K. Burke, and M. Ernzerhof, Generalized Gradient Approximation Made Simple, Phys. Rev. Lett. **77**, 3865 (1996).

[40] A. I. Liechtenstein, V. I. Anisimov, and J. Zaanen, Density-functional theory and strong interactions: Orbital ordering in Mott-Hubbard insulators, Phys. Rev. B **52**, 5467(R) (1995).

[41] H. O. Jeschke, F. Salvat-Pujol, and R. Valentí, First-principles determination of Heisenberg Hamiltonian parameters for the spin-$\frac{1}{2}$ kagome antiferromagnet $ZnCu_3(OH)_6Cl_2$, Phys. Rev. B **88**, 075106 (2013).

[42] D. Guterding, R. Valentí, and H. O. Jeschke, Reduction of magnetic interlayer coupling in barlowite through isoelectronic substitution, Phys. Rev. B **94**, 125136 (2016).

[43] P. Elliott, J. Brugger, A. Pring, M. L. Cole, A. C. Willis, and U. Kolitsch, Birchite, a new mineral from Broken Hill, New South Wales, Australia: Description and structure refinement, Am. Mineral. **93**, 910 (2008).

[44] Y. Iqbal, T. Müller, K. Riedl, J. Reuther, S. Rachel, R. Valentí, M. J. P. Gingras, R. Thomale, and H. O. Jeschke, Signatures of a gearwheel quantum spin liquid in a spin-$\frac{1}{2}$ pyrochlore molybdate Heisenberg antiferromagnet, Phys. Rev. Mater. **1**, 071201(R) (2017).

[45] L. Heinze, H. O. Jeschke, I. I. Mazin, A. Metavitsiadis, M. Reehuis, R. Feyerherm, J.-U. Hoffmann, M. Bartkowiak, O. Prokhnenko, A. U. B. Wolter *et al.*, Magnetization Process of Atacamite: A Case of Weakly Coupled $S = 1/2$ Sawtooth Chains, Phys. Rev. Lett. **126**, 207201 (2021).

[46] H. Yamamoto, T. Sakakura, H. O. Jeschke, N. Kabeya, K. Hayashi, Y. Ishikawa, Y. Fujii, S. Kishimoto, H. Sagayama, K. Shigematsu *et al.*, Quantum spin fluctuations and hydrogen bond network in the antiferromagnetic natural mineral henmilite, Phys. Rev. Mater. **5**, 104405 (2021).

[47] S. Blundell, *Magnetism in Condensed Matter*, Oxford Master Series in Condensed Matter Physics (Oxford University Press, Oxford, 2001).

[48] K. Iida, H. K. Yoshida, A. Nakao, H. O. Jeschke, Y. Iqbal, K. Nakajima, S. Ohira-Kawamura, K. Munakata, Y. Inamura, N. Murai *et al.*, $q = 0$ long-range magnetic order in centennialite $CaCu_3(OD)_6Cl_2 \cdot 0.6D_2O$: A spin-1/2 perfect kagome antiferromagnet with J_1-J_2-J_d, Phys. Rev. B **101**, 220408(R) (2020).

[49] S. Chillal, Y. Iqbal, H. O. Jeschke, J. A. Rodriguez-Rivera, R. Bewley, P. Manuel, D. Khalyavin, P. Steffens, R. Thomale, A. T. M. N. Islam *et al.*, Evidence for a three-dimensional quantum spin liquid in $PbCuTe_2O_6$, Nat. Commun. **11**, 2348 (2020).

[50] S. R. White and I. Affleck, Dimerization and incommensurate spiral spin correlations in the zigzag spin chain: Analogies to the Kondo lattice, Phys. Rev. B **54**, 9862 (1996).

[51] G. A. Bain, and J. F. Berry, Diamagnetic Corrections and Pascal's Constants, J. Chem. Educ. **85**, 532 (2008).

[52] W. Zheng, R. R. P. Singh, R. H. McKenzie, and R. Coldea, Temperature dependence of the magnetic susceptibility for triangular-lattice antiferromagnets with spatially anisotropic exchange constants, Phys. Rev. B **71**, 134422 (2005).

[53] J. H. Brewer, S. R. Kreitzman, D. R. Noakes, E. J. Ansaldo, D. R. Harshman, and R. Keitel, Observation of muon-fluorine "hydrogen bonding" in ionic crystals, Phys. Rev. B **33**, 7813(R) (1986).

[54] H. Boutin, G. J. Safford, and H. R. Danner, Low-Frequency Motions of H_2O Molecules in Crystals, J. Chem. Phys. **40**, 2670 (1964).

[55] H. Prask and H. Boutin, Low-Frequency Motions of H_2O Molecules in Crystals. II, J. Chem. Phys. **45**, 699 (1966).

[56] M. Månsson, Y. Ikedo, H. Nozaki, J. Sugiyama, P. L. Russo, D. Andreica, M. Shizuya, M. Isobe, and E. Muromachi, Muon spin relaxation study of misfit-layered cobalt dioxide $[Ca_{0.85}OH]^{RS}_{1.16}[CoO_2]$, Solid State Commun. **150**, 307 (2010).

[57] J. Sugiyama, Y. Ikedo, M. Månsson, J. H. Brewer, S. L. Stubbs, E. J. Ansaldo, K. H. Chow, J. S. Lord, H. Ohta, C. Michioka, and K. Yoshimura, Magnetic and superconducting nature of $Na_{0.35}CoO_2 \cdot yH_2O$ and $Na_{0.35}CoO_2 \cdot yD_2O$ investigated by muon-spin spectroscopy, Phys. Rev. B **82**, 214505 (2010).